JOURNAL OF APPLIED CRYSTALLOGRAPHY

Volume 54 (2021)

Supporting information for article:

Operando Structural Investigations of Thermoelectric Materials

Lasse Rabøl Jørgensen, Kasper Borup, Christian Moeslund Zeuthen, Martin Roelsgaard and Bo Brummerstedt Iversen

S1. Sample displacement

Figure S2 represents a geometrical depiction of the experimental setup. Position 1 (Pos 1) and 2 (Pos 2) indicates two arbitrary points on the sample, D is the distance from the Pos 2 to the detector and ΔD+D is the distance from Pos 1 to the detector. We subjectively chose to evaluate the peak shift of the diffraction peak present at $2\theta \approx 31.4$ ° since this is a non-overlapping high angle peak with appreciable intensity (the peak seen to the furthest right in the inset on Figure S1). This point on the detector corresponds to a real-space distance from the beam center of approximately 305 mm. The scattering angle of the two positions can be stated as follows:

$$2\theta_2 = \tan^{-1}\left(\frac{x}{D}\right) \quad 2\theta_1 = \tan^{-1}\left(\frac{x}{D + \Delta D}\right)$$

The difference in scattering angle as a function of sample displacement is then:

$$2\theta_2 - 2\theta_1 = \Delta 2\theta(\Delta D) = \tan^{-1}\left(\frac{305\ mm}{500\ mm}\right) - \tan^{-1}\left(\frac{305\ mm}{500\ mm + \Delta D}\right)$$

This function is visualized in Figure S2b. No apparent peak shift is observed from Figure S1 within the angular resolution of the instrument. The dotted line in Figure S2b indicates the angular resolution along with the corresponding sample displacement, which is less than 0.2 mm.

S2. Design considerations and material choices

S2.1. Materials

Successfully mimicking the conditions found in a TE module requires elevated temperatures and direct current. In ATOS, heat is supplied via the temperature-controlled brass blocks and current is delivered through the stainless steel tower, brass element, and across the sample. Apart from being stable at these conditions, the brass blocks also have a high thermal and electrical conductivity, which are necessary to efficiently transfer heat and current to the sample. We designed the brass blocks to have a high thermal mass while still being able to dissipate heat to the surroundings quickly. This combination makes the brass blocks act as both good heat reservoirs for the hot end and heat sinks for the cold end, which makes the temperature easily controllable and stable. In addition, brass is very inexpensive and easy to machine, making it an ideal material for this purpose. However, one should be aware of compounds reacting with the brass elements, such as $Cu_{2-x}Se$. In these cases, an electron-conducting layer (e.g. graphite paper) is inserted between the sample and the brass block. For very high temperature applications, brass is not ideal since it is readily oxidized above 700 K.

S2.2. Nickel probes

Two nickel probes are placed in contact with the top surface of the sample. Here, good electrical contact between the sample and the probes is important, as a poor contact will result in increased contact resistance and increased measurement noise. A range of metals such as Ni, Mo, Nb, W and some alloys are suitable, but due to the high inertness, appropriate flexibility and availability, Ni was chosen despite having a high Seebeck coefficient of approximately -20 μV/K. To avoid signals from the Ni probes appearing in the diffraction data and avoid excessively perturbing the temperature gradient along the sample, the probes are contacting the sample either above or close to the brass blocks.

S2.3. Sample preparation

To obtain high-quality powder X-ray diffraction patterns, the orientation of the crystallites in the illuminated sample must be random. A tendency for the crystallites to favor certain orientations will result in grainy Debye-Scherrer cones on the detector leading to erroneous peak intensities and profiles. In regular PXRD experiments performed on finely powdered samples in capillaries, this is avoided to a large extent by continuously spinning the sample. The ATOS does not allow for sample rotation, and samples have to be compacted using sintering pressing tools to obtain a sufficient density of at least 95 % of the crystallographic density. Some crystallite alignment is expected in samples, which have been densified using a hot press or spark plasma sintering press, and extensive sintering furthermore tends to promote crystal-lite growth. As such, it is important to 1) reduce the crystallite size of the starting materials before the sintering, 2) reduce the sintering temperature as much as possible while still obtaining sufficiently dense samples, and 3) reduce the sintering time as much as possible. These obstacles can be largely mitigated by milling and sieving the synthesized materials prior to pressing and by careful optimization of the sintering conditions.

The interaction between X-rays and condensed inorganic matter is relatively strong and for X-ray diffraction experiments in transmission geometry, absorption of the X-rays by the sample is an important consideration as this will reduce the intensity of the scattered beam and possibly introduce complications in the data analysis. The absorption of X-rays is calculated from the absorption coefficient, μ, which depends on X-ray energy-specific absorption cross-section for the material as well as the sample density (Als-Nielsen & McMorrow, 2011). The samples possess higher density than normal powder samples and often consist of heavy elements such as Sb, Bi and Te, which pose severe re-strictions on the sample thickness. As a rule of thumb, the thickness of the sample, t, should be chosen such that $\mu t < 4.0$ (McCusker *et al.*, 1999). On the other hand, reducing the sample thickness too much will reduce the effective thermal conductance of the sample resulting in a steeper and more uncertain thermal gradient across the sample. The samples included in this study are cut into bars of 1 mm x 1 mm x 10 mm, which is the upper thickness limit for the applied X-ray energy of 60 keV. The maximum

sample length is about 25 mm, which is the maximum separation of the two towers. The minimum sample length depends on 1) the desired overlap between the sample and the tower, where a larger overlap yields a better thermal contact. 2) The desired thermal gradient, where a longer distance between the towers will give a larger thermal gradient. 3) The number of points of investigation on the sample.

S2.4. Picking the right system

The kinetics of the reaction of interest obviously have to be resolvable with the time resolution of the measure-ment in order to be observed. Depending on the data acquisition mode, ATOS has a lower time resolution boundary of approximately 1 second, which might be decreased by increasing the photon flux of the X-ray source. Therefore, it is currently not possible to observe reactions occurring on the sub-second time scale. On the other hand, slow reaction kinetics can also be a disadvantage as the experimental time has to fit within the period of a synchrotron beamtime, which is usually a few days. However, for longer experiments, the setup can be installed in-house without the structural probing by X-rays, and then only electrical resistance and Seebeck coefficient are obtained during the experiment.

The ATOS initially was built for testing thermoelectric materials, but it should be stressed that it can also be used for solving challenges in other fields of materials science, where the materials are exposed to a high temperature, temperature gradient or an electric field.

S2.5. Operation

A typical experiment would commence by locating the outer boundaries of the sample by translating the setup perpendicular to the beam. The sample is then centered in the beam by translating the setup vertically. For data acquisition, two different modes are employed based on the scientific case. In the first mode, the sample can be cyclically translated perpendicular to the direct beam to specific positions. This gives spatial information with the expense of a decreased time resolution at each position. Alternatively, data is acquired at a fixed position with a time-resolution of approximately 1 second, compared to minutes for cyclic translation. The data acquisition method should therefore be chosen based on the kinetics of the reaction of interest. Before initializing external parameters, diffraction data is collected at different points along the sample to ensure structural homogeneity.

S3. Testing ATOS

S3.1. Perpendicularity

Since a varying sample-to-detector distance will be reflected in the refined unit cell parameters, a certified NIST standard sample can be used to quantify the sample displacement. In practice, this is

done by loading LaB_6 (NIST 660b) powder into a 1.0 mm outer diameter kapton capillary, mounting the capillary in the ATOS and collecting X-ray diffraction data at various positions along the sample by translating the setup perpendicular to the beam. The refined unit cell parameters can be seen in Figure S3. The variation in the refined unit cell parameter is on the order of 10^{-4} Å, which defines the uncertainty with which unit cell parameters can be compared between different points in the ATOS. From geometrical considerations, the shift in diffraction peak position as a function of sample displacement along the beam path is most pronounced at higher angles. In the present case, a comparison of the high-angle region of the raw diffraction patterns collected at each end of the sample shows no visible peak shift within the angular resolution of the experiment (Figure S1). Thus, if the diffraction peak at $2\theta \approx 31.4°$ ($Q \approx 16.4$ Å-1), comprised of the (10 3 3) and (9 6 1) reflections, is shifted less than the angular resolution of 0.01° between the two data sets, an estimated sample displacement of less than 0.2 mm from end to end is obtained, as shown earlier. For the actual samples, a thickness deviating from 1.0 mm will increase the uncertainty of the absolute value of the refined unit cell parameter since the sample-to-detector distance is calibrated using a 1.0 mm thick LaB_6 sample. The sample perpendicularity is further ensured through a high-precision camera mounted directly above the sample during operation, as is shown in Figure S13.

S3.2. Separating heat and current

Our initial operando setup had no active heating source. Instead, due to the applied high currents and the limited possibility for the system to discard heat, severe Joule heating was observed, thereby irrevocably linking the current and temperature effects, making any separation difficult. In ATOS, the brass elements, on which the sample is mounted, are designed to act as heat sinks, effectively receiving much of the thermal energy released in the sample during resistive heating. Exposing β-Zn_4Sb_3 to a current density of 1.14 A/mm^2 in the first operando setup resulted in severe migration of Zn-ions along the direction of the current, which eventually resulted in decomposition of β-Zn_4Sb_3 into ZnSb in the Zn-deficient end of the sample after approximately 55 minutes. In order to compare the new setup to the old one, the experiment was repeated using ATOS, and the raw diffraction patterns are shown in Figure 2a. During this experiment, diffraction data is measured at the end where Zn-ions accumulate. After approximately 120 minutes of exposure to the DC current, no secondary Zn phase is observed and the β-Zn_4Sb_3 phase appears unchanged. Figure S4 shows the refined unit cell parameter for β-Zn_4Sb_3 along with the temperature of the brass element. The unit cell parameter increases immediately due to the rapid Joule heating caused by the DC current. The unit cell parameter then slowly falls while the temperature of the brass block correspondingly increases. This clearly demonstrates the ability of the brass block to accept heat from the sample. The spike in unit cell size observed immediately after the current is turned on is expected to originate from the con-tact resistance between the sample and the

tower. This resistance can be a factor of 10-100 larger than the electrical resistance of the sample causing excessive Joule heating in the contact region. This local annealing seems to improve the contact resistance over time, which is reflected in the subsequently decreasing unit cell size.

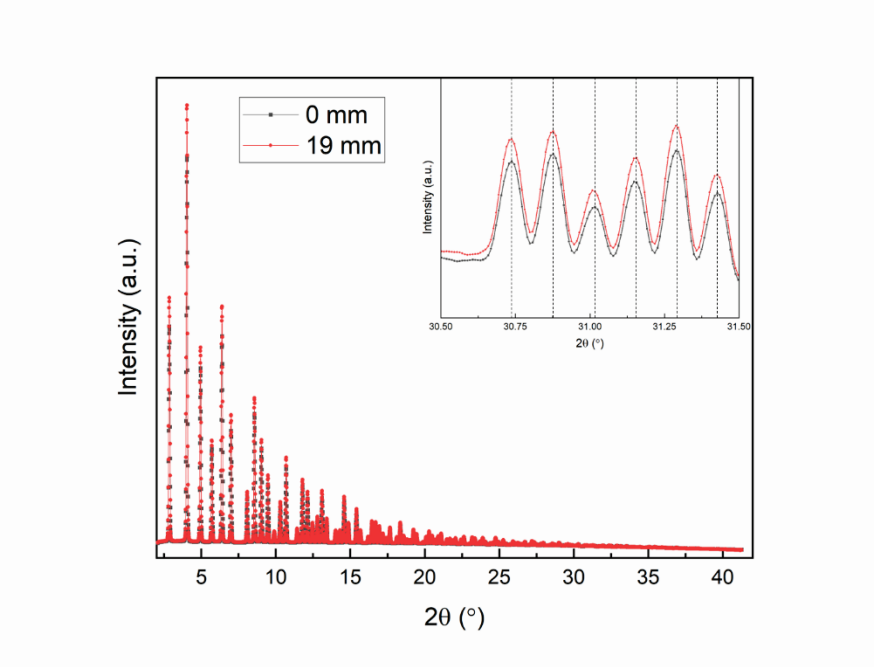

Figure S1 X-ray diffraction patterns collected on a LaB_6 standard sample packed in a 1.0 mm diameter capillary. The two patterns are collected at each end of the capillary spaced 19 mm apart. The inset shows a high angle region, where the peak positions in the two patterns are equal.

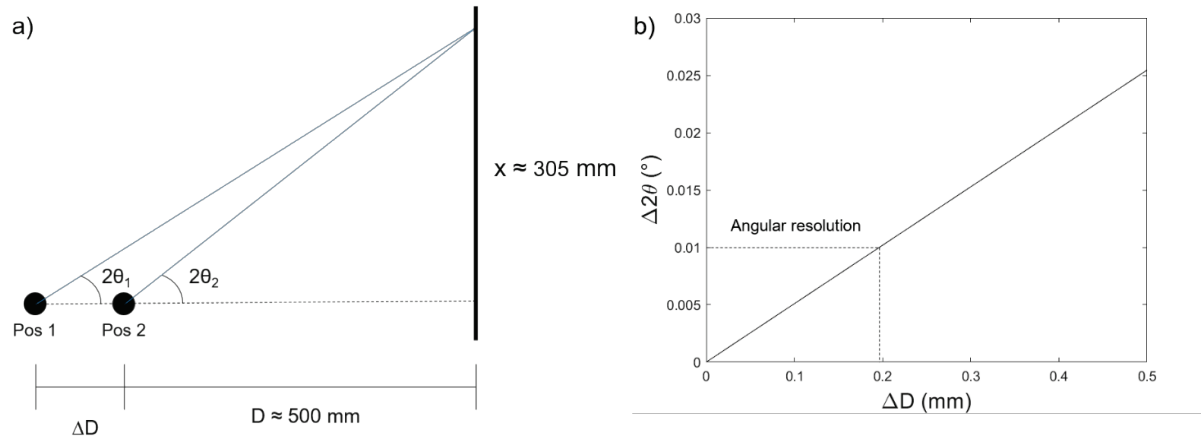

Figure S2 a) Geometrical depiction of the experimental setting. b) The difference in scattering angle as a function of sample displacement.

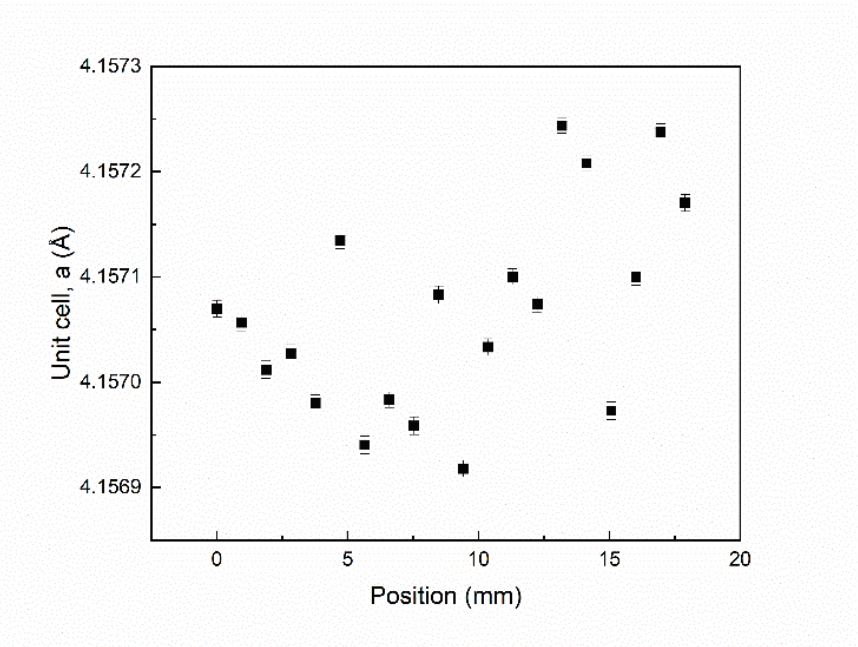

Figure S3 Refined unit cell parameter for LaB6 NIST standard collected at several positions along the length of the sample.

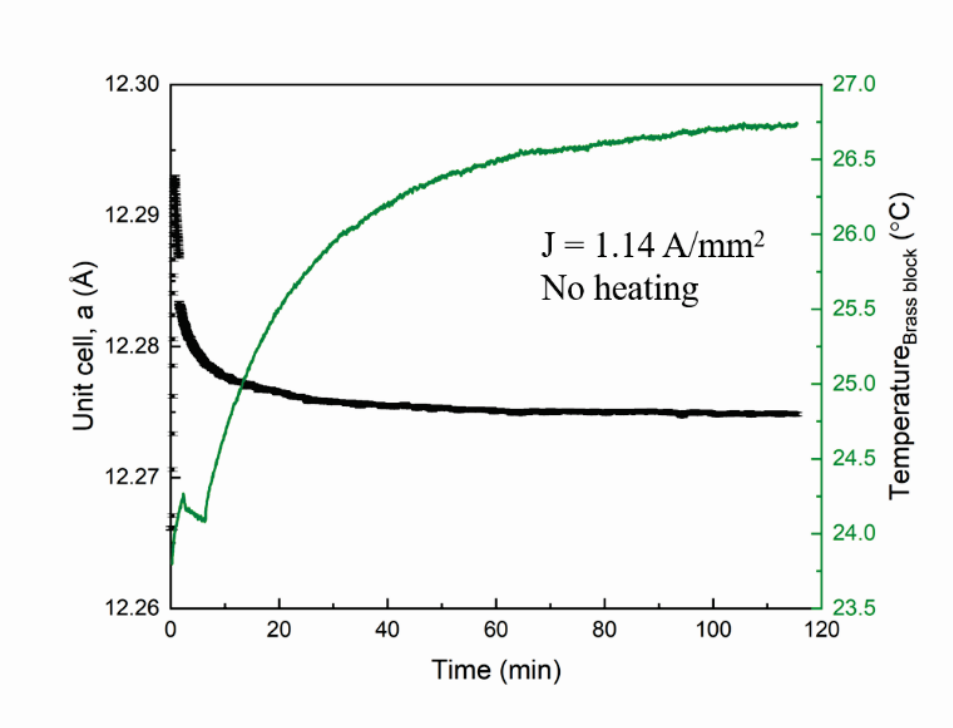

Figure S4 Refined unit cell parameter for β-Zn4Sb3 along with the temperature of the brass block.

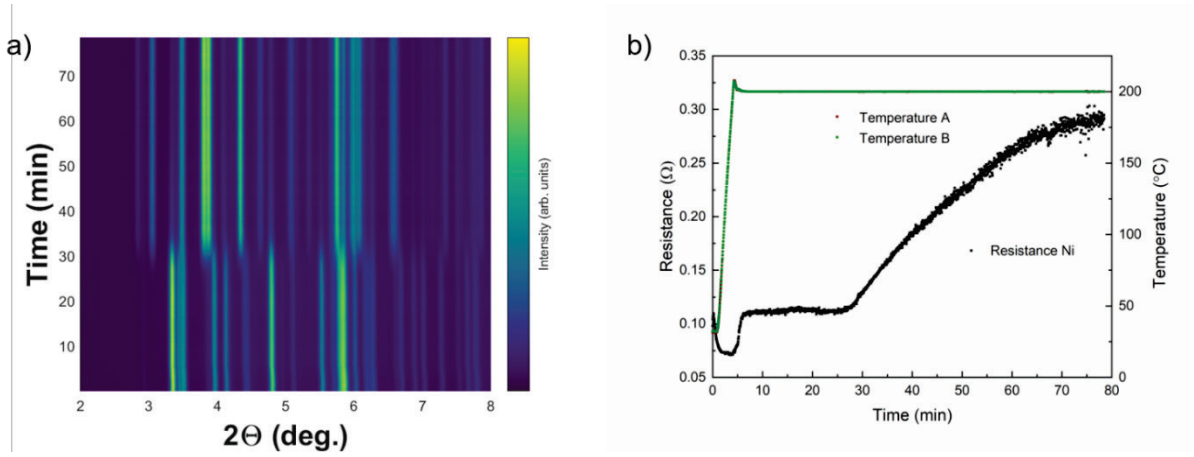

Figure S5 a) Raw diffraction patterns collected on at the end where the current enters the sample. b) Experimental temperature along with the measured electrical resistance.

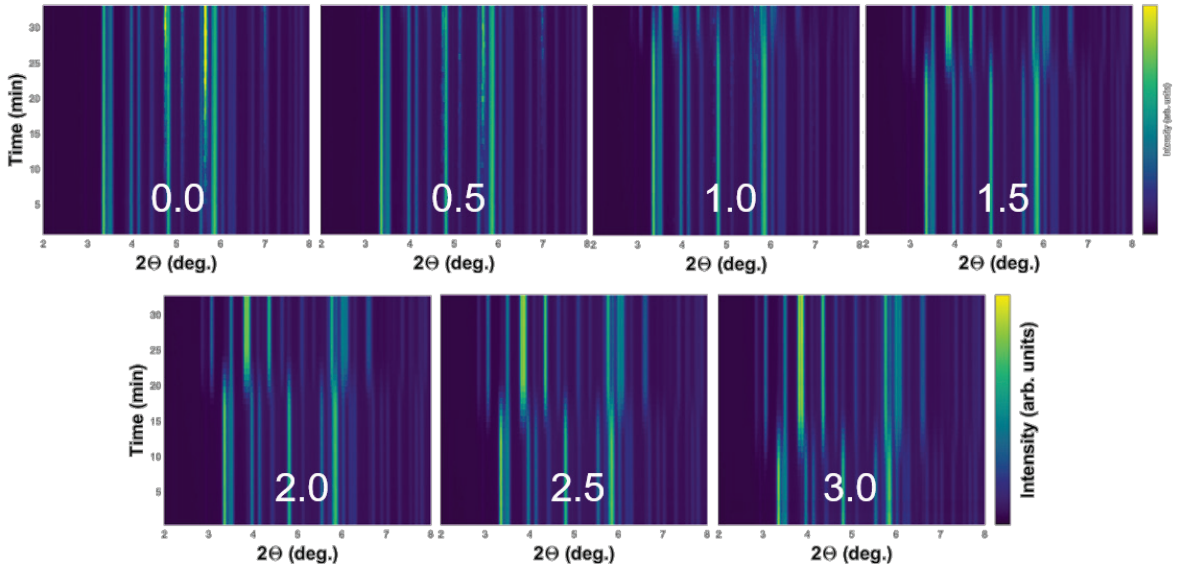

Figure S6 Raw X-ray diffraction patterns collected at different positions along the sample throughout the experiment.

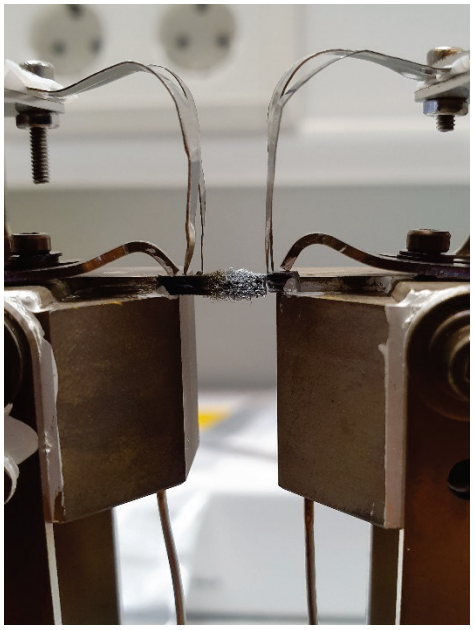

Figure S7 Picture of a Zn4Sb3 sample taken after experiment.

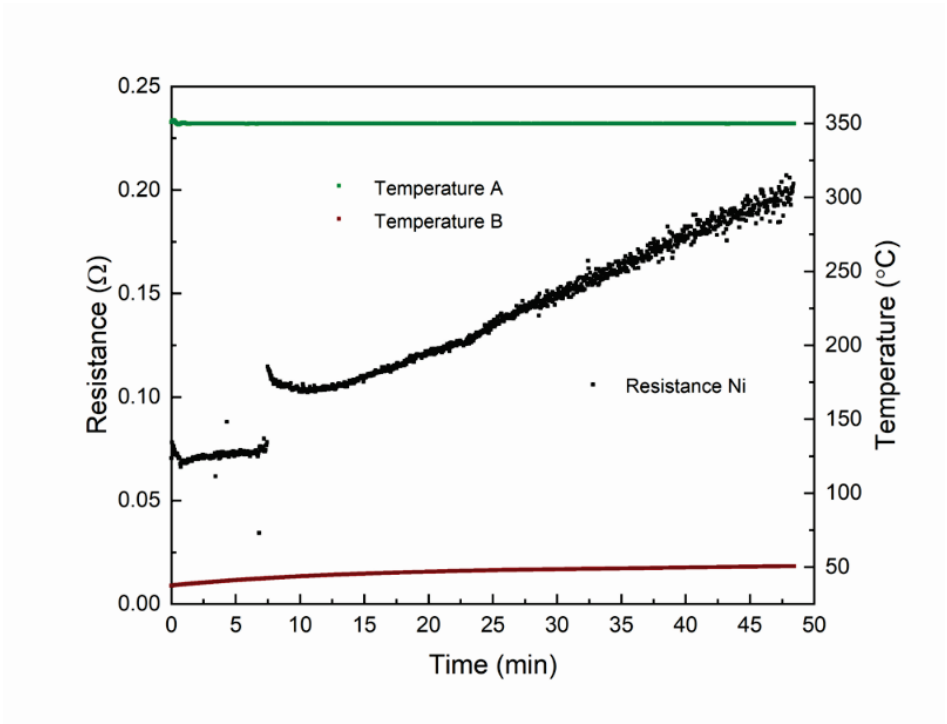

Figure S8 Experimental temperature of the two towers along with the measured electrical resistance.

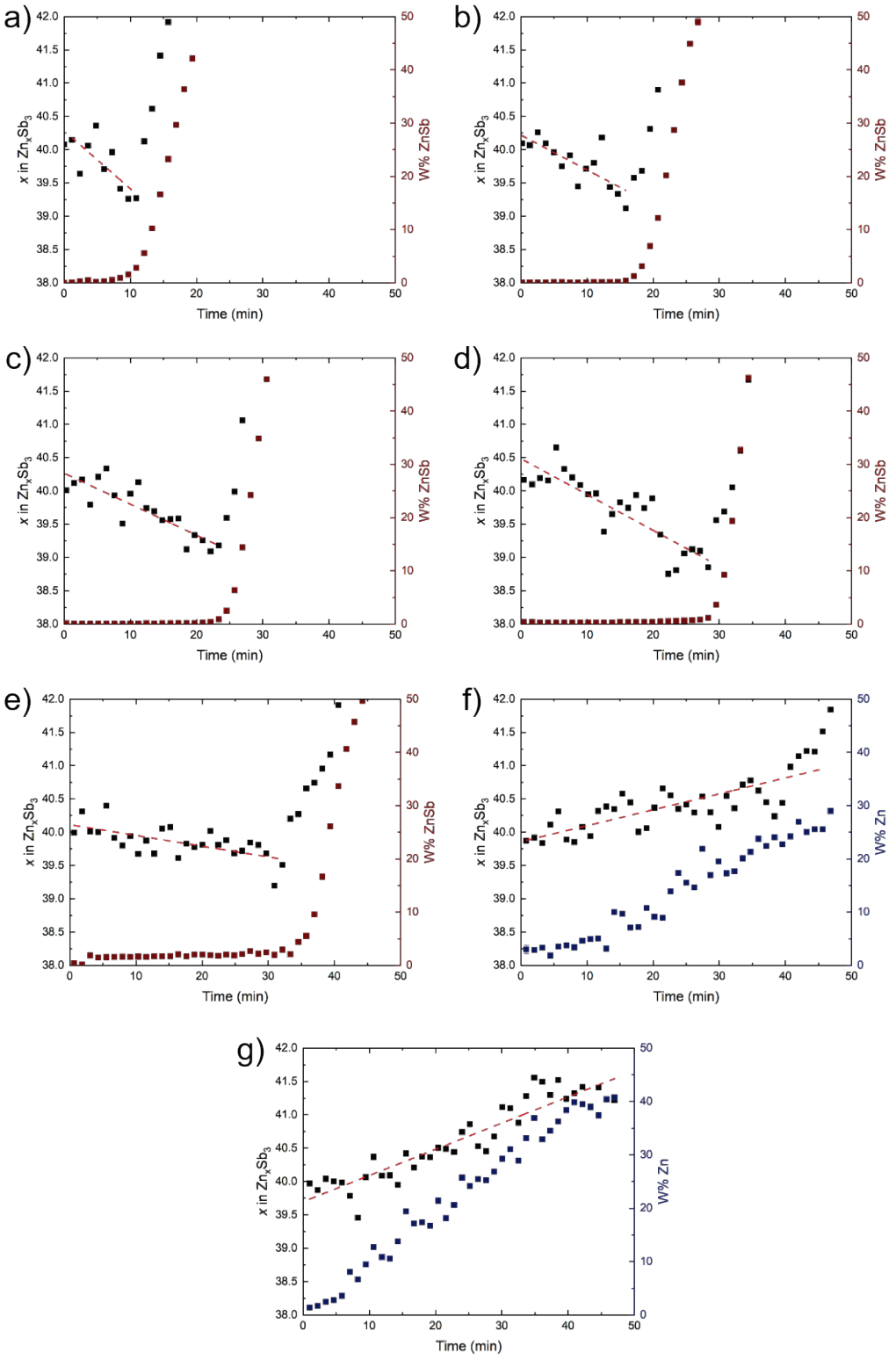

Figure S9 Atomic composition of the β-Zn4Sb3 phase as a function of time plotted together with the weight fraction of the secondary phase. A linear regression is fitted to the composition as a function of time (red dashed line) up until a secondary phase appears. The investigated positions of the sample ranges from 0.0 mm (a) to 3.0 mm (g) in steps of 0.5 mm. The hot side of the sample is at 3.0 mm.

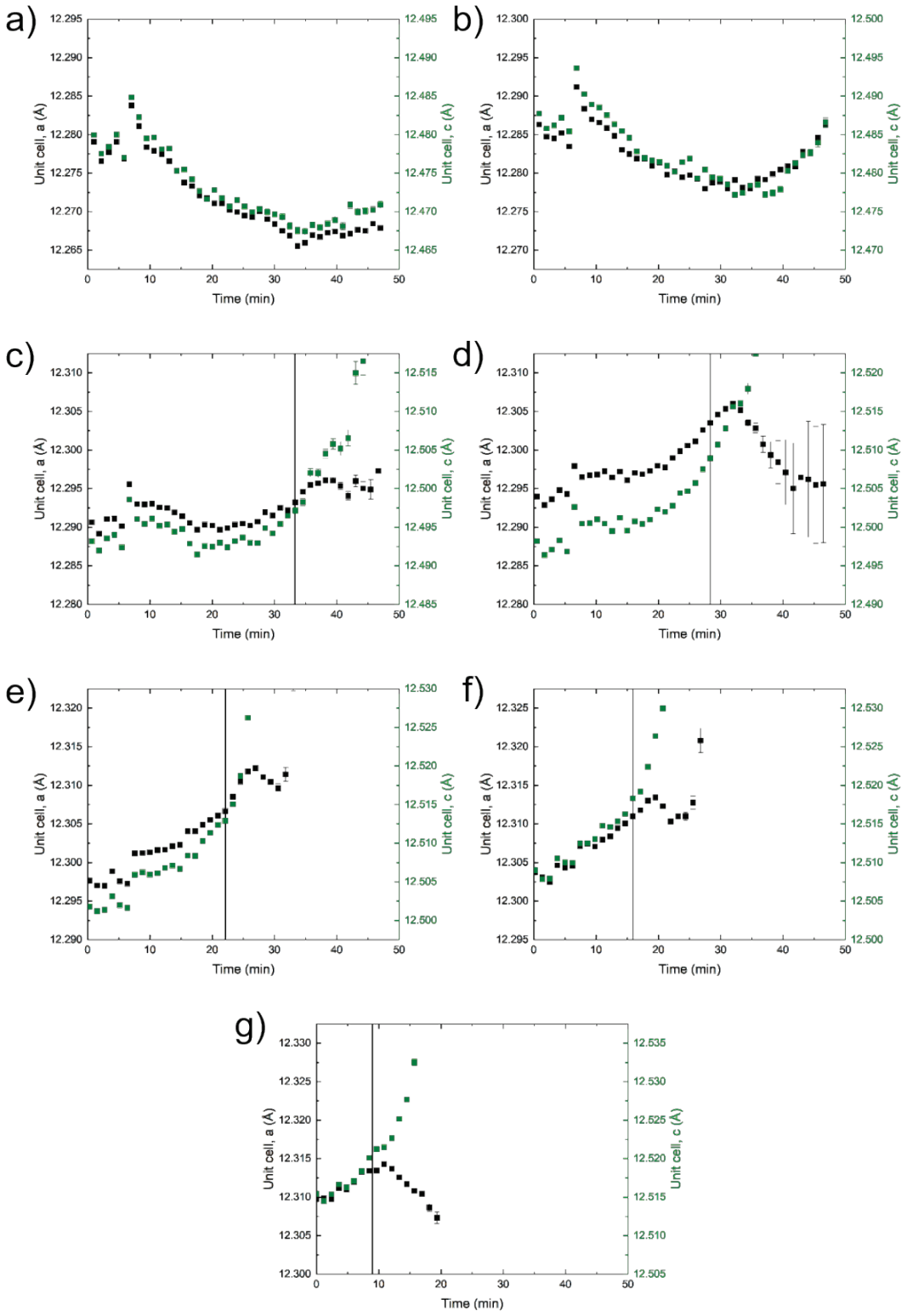

Figure S10 Refined unit cell parameters for β-Zn4Sb3 exposed to a thermal gradient and external current in the forward bias. The vertical black line indicates the point of decomposition. The investigated positions of the sample ranges from 0.0 mm (a) to 3.0 mm (g) in steps of 0.5 mm. The hot side of the sample is at 3.0 mm.

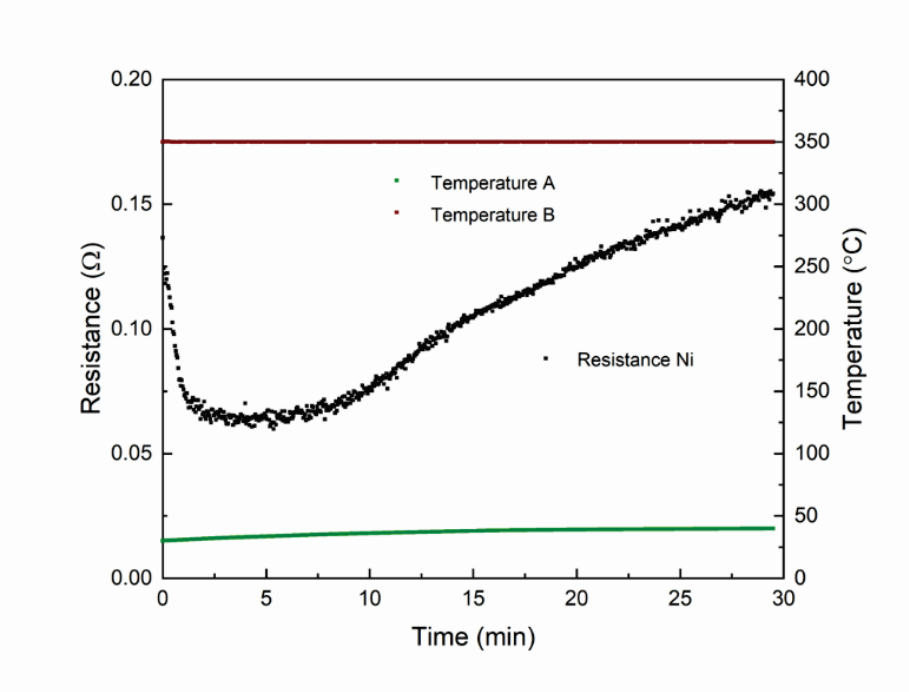

Figure S11 Experimental temperature of the two towers along with the measured electrical resistance.

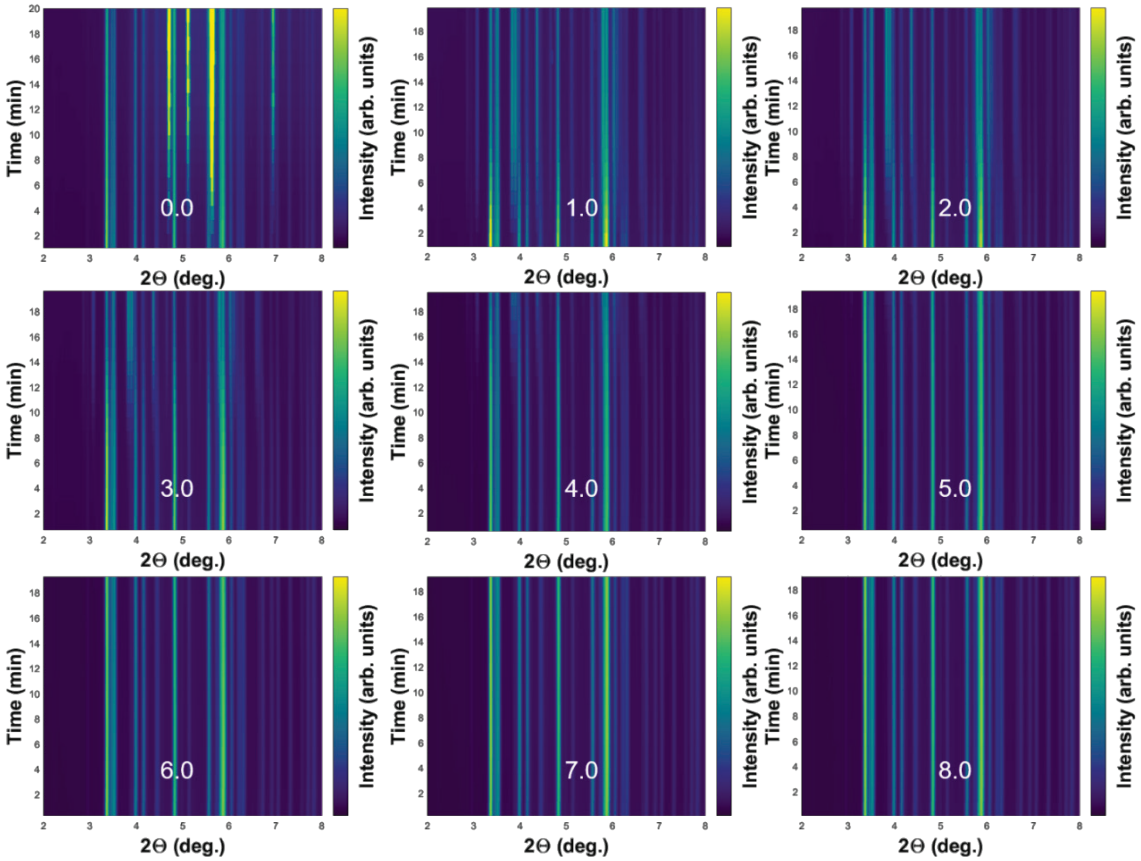

Figure S12 Raw X-ray diffraction patterns collected at different positions along the sample throughout the experiment.

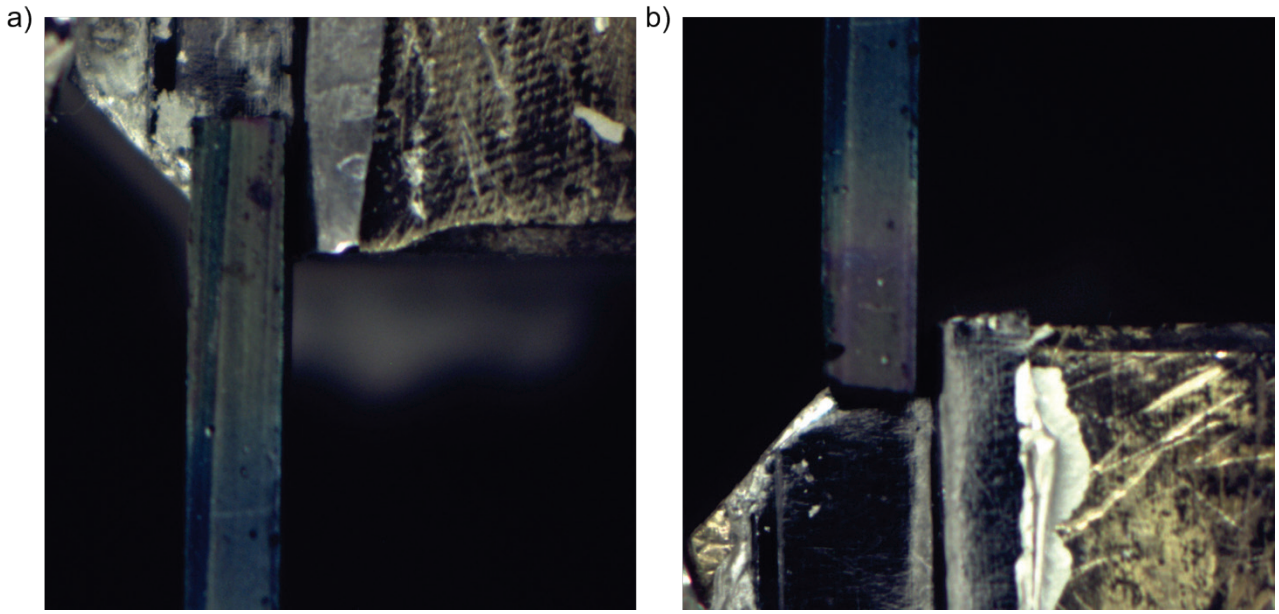

Figure S13 Pictures of the a) cold side and b) hot side of the sample seen from above.

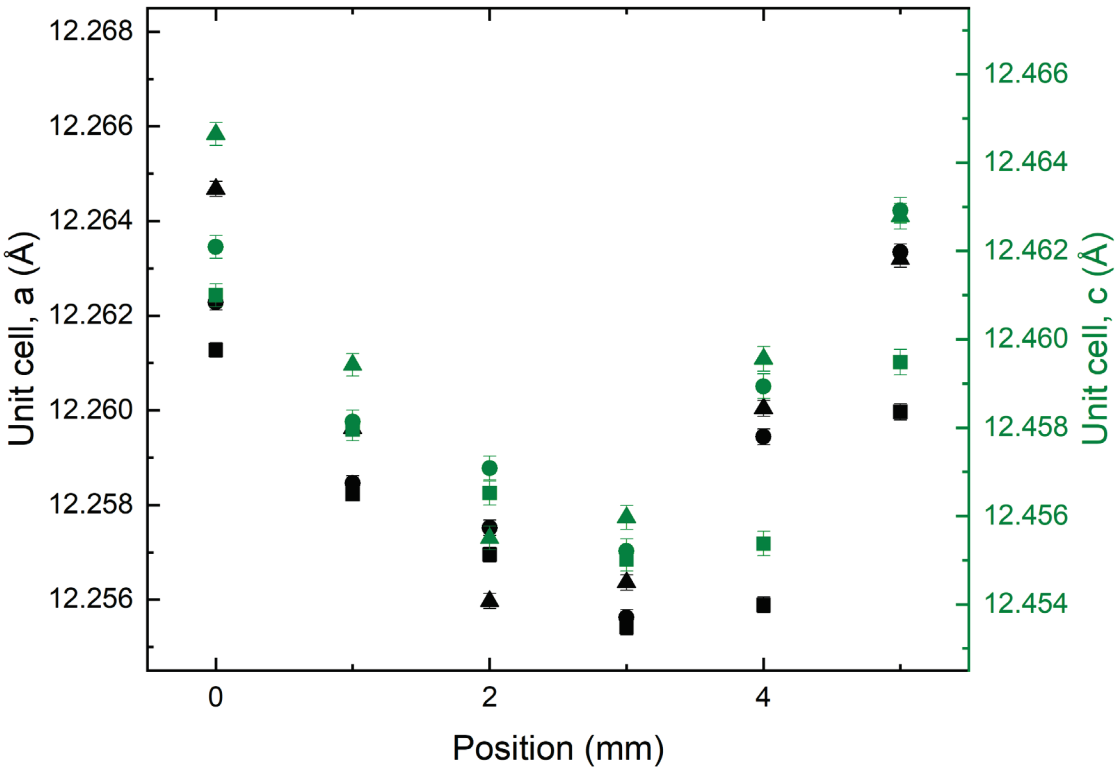

Figure S14 The temperature landscape along the sample displayed through the unit cell parameters of β-Zn_4Sb_3. Three scans along the sample has been included with separate scatter symbols. The temperature of each tower is set to 250 °C.

References

Als-Nielsen, J. & McMorrow, D. (2011). Elements of Modern X-ray Physics Wiley.

McCusker, L. B., Von Dreele, R. B., Cox, D. E., Louër, D. & Scardi, P. (1999). *J. Appl. Crystallogr.* **32**, 36–50.